

By acceptance of this article, the publisher or recipient acknowledges the U.S. Government's right to retain a nonexclusive, royalty-free license in and to any copyright covering the article.

**DRAFT**

**PLASMA ENGINEERING ANALYSIS OF TENNESSEE TOKAMAK\***

**K. E. Yokoyama, J. T. Lacatski, and J. B. Miller**  
University of Tennessee  
Department of Nuclear Engineering  
Knoxville, Tennessee 37916

**W. E. Bryan, P. W. King, R. T. Santoro, T. E. Shannon, and N. A. Uckan**  
Oak Ridge National Laboratory  
Oak Ridge, Tennessee 37831

CONF-831203--55-Draft

CONF-831203--55-Draft

DE84 004692

\*Research sponsored by the Office of Fusion Energy, U.S. Department of Energy, under contract No. W-7405-ENG-26 with Union Carbide Corporation.

**DISCLAIMER**

This report was prepared as an account of work sponsored by an agency of the United States Government. Neither the United States Government nor any agency thereof, nor any of their employees, makes any warranty, express or implied, or assumes any legal liability or responsibility for the accuracy, completeness, or usefulness of any information, apparatus, product, or process disclosed, or represents that its use would not infringe privately owned rights. Reference herein to any specific commercial product, process, or service by trade name, trademark, manufacturer, or otherwise does not necessarily constitute or imply its endorsement, recommendation, or favoring by the United States Government or any agency thereof. The views and opinions of authors expressed herein do not necessarily state or reflect those of the United States Government or any agency thereof.

**NOTICE**  
**PORTIONS OF THIS REPORT ARE UNLEGIBLE.**  
It has been reproduced from the best available copy to permit the broadest possible availability.

DISTRIBUTION OF THIS DOCUMENT IS UNLIMITED

*EJB*

This paper summarizes the results of the plasma engineering and systems analysis studies for the Tennessee Tokamak (TENTOK) fusion power reactor. TENTOK is a 3000-MW(t) central station power plant that uses deuterium-tritium fuel in a D-shaped tokamak plasma configuration with a double-null poloidal divertor. The major parameters are  $R_0 = 6.4$  m,  $a = 1.6$  m,  $\sigma$ (elongation) = 1.65,  $\langle n \rangle = 1.5 \times 10^{20} \text{ m}^{-3}$ ,  $\langle T \rangle = 15$  keV,  $\langle \beta \rangle = 6\%$ ,  $B_T$  (on axis) = 5.6 T,  $I_p = 8.5$  MA, and wall loading = 3 MW/m<sup>2</sup>. Detailed analyses are performed in the areas of (1) transport simulation using the 1-1/2-D WHIST transport code, (2) equilibrium/poloidal field coil systems, (3) neutral beam and radiofrequency (rf) heating, and (4) pellet fueling. In addition, impurity control systems, diagnostics and controls, and possible microwave plasma preheating and steady-state current drive options are also considered. Some of the major features of TENTOK include rf heating in the ion cyclotron range of frequencies, superconducting equilibrium field coils outside the superconducting toroidal field coils, a double-null poloidal divertor for impurity control and alpha ash removal, and rf-assisted plasma preheating and current startup.

### Introduction

The Tennessee Tokamak (TENTOK) design effort has been concentrated on a plasma engineering analysis of the reactor system extending to the first wall [1]. Innovative and new ideas in physics and technology were investigated; such as the possibility of using a beam-shaped plasma to gain access to the "second stability" regime, the possibility of steady-state (or very long pulse) current drive, and rf-assisted start-up. Because the design of the systems outside the first wall was not considered in detail, typical system parameters (such as blanket and shield thickness, number of coils, maximum field and coil current density, etc.) were chosen based on current technological developments and other similar studies. The typical TENTOK parameters are summarized in Table I.

An analysis of magnetics, MHD equilibrium, particle and energy transport, heating and fueling, and impurity control has been made to support the plasma parameters specified in Table I. The TENTOK plasma should achieve and ignited burn of deuterium-tritium fuel with a total fusion power output of 3000 MW(t). Designed on a smaller scale than STARFIRE [2], TENTOK has a plasma

minor radius of 1.6 m, a major radius of 8.45 m, and a plasma elongation of 1.65. The plasma current is in excess of 8.5 MA, which is adequate to confine alpha particles. Operation at low safety factor  $q$  at the plasma edge,  $q(a) \leq 2.5$ , is sought in order to obtain high values of  $\langle \beta \rangle \approx 6\%$  and low plasma disruptivity. With respect to obtaining high-beta, the use of bean-shaped plasmas are also considered. Although bean-shaped configurations offer the possibility of having an access to the second stability regime, a dee-shaped plasma is chosen for TENTOK. The primary reasons for not considering the bean-shaped plasma were as follows: (1) for proper plasma shaping, inboard poloidal field coils are required inside the blanket-shield assembly making the use of superconducting coils impractical and maintenance difficult, (2) the resulting scrape-off region is so thin that the use of a pumped limiter or poloidal divertor would be difficult, and (3) a very high plasma current is required.

Assuming a 20% efficiency, the 125 MW of neutral beam heating power at 200 keV allows the plasma to be heated to ignition for energy losses up to about two-to-three times as large as the present estimates for heat conduction primarily derived from empirical Alcator scaling. Neo-Alcator scaling and empirical "H-mode" scaling are also considered. The possibility of rf heating at the ion cyclotron range of frequencies (ICRF), especially at the second harmonic of bulk-plasma deuterons ( $\omega_{rf} = 2 \Omega_D$ ), is also investigated. The fueling system consists of a gas puffing system and a pellet injection system. The pellets are 3 mm radius injected at 2 km/s. A double-null poloidal divertor has been chosen for impurity control and particle handling.

In the remaining of this paper, we discuss the major design characteristics, plasma performance estimates, heating and fueling options, impurity control and particle handling, and diagnostics and controls for TENTOK.

#### Characteristic TENTOK Parameters and Plasma Shape

A physics systems code is developed to consider both physics and engineering constraints from which a consistent set of reactor parameters is calculated for the TENTOK (see Table I). Considered in the analysis are (1) various scaling laws governing energy transport, (2) stability constraints ( $\beta$ -limits) associated with various external and internal modes (kink, ballooning,

disruption, etc.), (3) magnetics requirements, and (4) power balance. The technology and engineering requirements are also considered, but only to the extent required to ensure that no obvious engineering constraints are being violated.

The detailed calculations are carried out for a 3000 MW(t) reactor with a neutron wall loading of  $3 \text{ MW/m}^2$ . The operating temperature at ignition is chosen to be around 15 keV to maximize the reactivity,  $\langle \sigma v \rangle / T^2$ . Considerations of stability (beta limits), equilibrium, magnetics, low plasma disruptivity led to the selection of plasma elongation  $\sigma = 1.65$ , safety factor at the plasma boundary  $q(a) \approx 2.5$ , and burn average plasma beta  $\langle \beta \rangle \approx 6\%$ . The remaining parameters are listed in Table I and the computational details are given in Ref. [1].

TENTOK's poloidal field coil system has been selected to satisfy MHD equilibrium requirements imposed by a double-null poloidal divertor and plasma position/shape control. Equilibrium solutions are generated for plasmas with "D" and "bean" shapes. Figure 1 shows the equilibrium poloidal field contours (surfaces of constant total flux) for (a) D-shaped plasma with a double-null poloidal divertor and (b) bean-shaped plasma (without a divertor). Although potential for high beta [about 14% for the case shown in Fig. 1(b)] exists for a bean-shaped plasma, because of the requirements of inboard poloidal field coils and very high plasma current (>15 MA), a D-shaped plasma [Fig. 1(a)] is considered for TENTOK. The parameters of the final equilibrium solution are nearly equivalent to the parameters specified in Table I (however, plasma current is somewhat higher and poloidal beta is somewhat lower).

### Plasma Performance Analysis

Transport calculations have been carried out for TENTOK plasma to determine heating (neutral beam and ICRF) and pellet fueling requirements and to access its performance and sensitivity to (1) various transport scaling models, (2) prompt and diffusive loss of alpha particles, (3) losses induced by toroidal field ripple, and (4) finite-beta-induced electron conduction losses. The POPCON option of the 1-1/2-D WHIST transport code [3] is used for these assessments.

The results of the WHIST code demonstrated the overall consistency of the TENTOK design model and

parameters given in Table I, as well as provided information as to the selection of proper transport model, heating power requirements, fast alpha loss constraints, and allowable toroidal field ripple variation.

The reference performance (Table I) was determined from the following transport model for electron ( $x_e$ ) and ion ( $x_i$ ) conduction [1]:

$$x_e = 3x_e^{NC} + 2x_e^{an} + x_e^{CD}$$

$$x_i = 3x_i^{NC} + x_i^{RT} + x_i^{BD}$$

where  $x_e^{NC}$  and  $x_i^{NC}$  are the neoclassical electron and ion conduction, respectively,  $x_e^{an} = 5 \times 10^{17}/n_e$  ( $\text{cm}^2/\text{s}$ ) is the anomalous contribution ("Alcator" scaling),  $x_e^{CD}$  is associated with enhanced electron thermal conduction (due to finite-beta) derived by Carreras-Diamond [4], and  $x_i^{RT}$  and  $x_i^{BD}$  are ion thermal conductances due to toroidal field ripple (RT due to ripple trapping [5] and BD due to banana drift [6]). Table II summarizes TENTOK base parameters and models used for POPCON plots.

Adequate fueling of the plasma core region was attained with 3 mm radius pellets injected at 2000 m/s. Further increases in injection velocity showed little impact.

Neutral beam (auxiliary) power contours for the TENTOK reference reactor are plotted in density-temperature space in Fig. 2. The local minima in density of the power contours and the saddle point define the thermally unstable region [3]. An optimal heating path (combined with optimal path to operating point) is also illustrated in Fig. 2, which passes through the saddle point and intersects the power contours at the points of minimum energy content (minimum beta points) above the saddle point and at maximum thermal energy content (maximum beta) below the saddle point. Once the ignition curve is intersected, it is followed up to the operating point. Superimposed on Fig. 2 are the total fusion (neutron plus alpha) power contours. (Blanket multiplication is not included.)

Figure 2 is based on the selection of a 200 keV deuterium beam energy with a source species mix by power at source of 80:12:8 ( $P_1:P_{1/2}:P_{1/3}$ ) for the full, half, and one-third energy components. This selection was made over that of a 150 keV or 175 keV beam energy due to better deposition of power. Figure 3 illustrates the

beam deposition  $[H(r)]$  profiles for the primary (full energy) components of 150 keV and 200 keV beams injected perpendicularly into the device.

Figure 4 illustrates the auxiliary heating contours for ICRF heating. The heating profile is taken to be a Gaussian,  $H(r) \sim \exp[-(2r/a)^2]$ , with 75% of the power delivered to the thermal ions. Since this model is independent of plasma density, reduced heating power requirements over that of neutral beams result above the saddle point. Both Figs 2 and 4 indicate that power is deposited in the plasma. Considering a neutral beam injector efficiency of 0.2 and assuming the same for the ICRF system (which is a pessimistic assumption for RF) the TENTOK requires a maximum of approximately 125 MW of auxiliary heating to reach ignition.

Shown in Fig. 5 are the contours of average toroidal and poloidal beta ( $\langle\beta_T\rangle$  and  $\langle\beta_p\rangle$ , respectively) and contours of constant  $Q$ , where  $Q = P_{\text{fus}}/P_{\text{beam}}$  ( $= P_{\text{fus}}/P_{\text{aux}}$ ), for the TENTOK reference model. At the operating point (ignition)  $Q = \infty$ . Contributions from fast beam ions and alphas are included in the total pressures. The average pressure contribution from fast alphas is  $\approx 18\text{--}20\%$  of the thermal plasma pressure near the operating point. At the operating point  $\langle\beta_T\rangle \approx 6.7\%$  and  $\langle\beta_p\rangle \approx 4.4\%$ .

Figure 6 indicates central ion and electron temperature contours. The hot ion mode characteristics of the TENTOK plasma is evident from the figure. For most of the density temperature space the central ion temperature is higher than the electron temperature.

Figure 7 shows the total energy confinement time contours. Reduced confinement is evident due to poor beam penetration at high  $\langle n_e \rangle$  and low  $\langle T \rangle$  and due to ripple conduction losses at intermediate  $\langle n_e \rangle$  and high  $\langle T \rangle$ . Energy confinement times in the ignition region are improved due to alpha heating. At the operating point,  $\tau_E \approx 1.0$  sec.

In addition to determining TENTOK neutral beam and/or ICRF heating requirements, Figs. 5-7 show the importance of the use of complete transport modeling in reactor design along with system integration studies. When the blanket multiplication factor of 0.25 is considered, Fig. 5 indicates a total fusion power of 2800  $[14.1 (1 + 0.25) + 3.52] = 3360$  MW(t), 12% higher than that considered in the systems analysis (see Table I). This is due partly to the fact that central ion temperature is of order 30 keV in the vicinity of the operating point (see Fig. 6) and  $T_i > T_e$ . The

enhanced fusion reaction rate, over that of assumed  $T_e \approx T_i$  with  $\langle T \rangle \approx 15$  keV in the systems analysis, accounts for the difference in fusion power. Likewise, the  $\langle \beta_T \rangle$  and  $\langle \beta_p \rangle$  are higher than that predicted in the systems design. In the transport calculations, as indicated earlier, contributions from fast beam ions and alphas are included in both  $\langle \beta_T \rangle$  and  $\langle \beta_p \rangle$ . Although at the ignited operating point fast beam ion pressure is zero, the alpha pressure is approximately 20% of the thermal pressure, an effect not included in the systems analysis. This especially impacts  $\langle \beta_p \rangle$ .

Figure 8 compares the neutral beam heating power contours for the TENTOK reference model with an alpha diffusion coefficient,  $D_\alpha$ , of  $1000 \text{ cm}^2/\text{sec}$  with an enhanced alpha diffusion case with  $D_\alpha = 5000 \text{ cm}^2/\text{sec}$ . Neutral beam power requirements greatly increased with the ignition region moving to higher densities in the enhanced alpha diffusion case to compensate for the loss of alpha heating capability.  $D_\alpha = 1000-2000 \text{ cm}^2/\text{sec}$  would be tolerable for the desired TENTOK reactor operating characteristics.

Similar sensitivity calculations have been carried out for enhanced (about a factor of 2 over the reference model) toroidal field ripple, anomalous, and finite-beta-induced transport losses. It is found that performance is not drastically degraded by an enhancement in only one group of losses (i.e., either in  $D_\alpha$ ,  $X_e$ ,  $X_i$ , or in  $X_e^{CD}$ ), however, for a combination of enhanced losses ignition may no longer be accessible in TENTOK.

### Plasma Heating and Fueling

Both neutral beam and ICRF heating are considered for the TENTOK. Plasma performance estimates for both schemes are discussed in the previous section. For the case of neutral beam heating the trade-off studies have been carried out to analyze the sensitivity of beam power and power supply requirements to changes in beam energy, beam species mix, and plasma parameters (density, temperature, and their profiles, along with the energy confinement time). Based on this trade-off, a beam energy of 200-keV is chosen for the TENTOK. The normalized beam deposition profiles,  $H_1(r)$ , for the full energy components of the 150 keV and 200 keV are shown in Fig. 3. This figure is for one of the POPCON sweeps that is a scan of constant, high density ( $\langle n \rangle \gtrsim 10^{14} \text{ cm}^{-3}$ ) with a constant rate of temperature

increase in time. It can be seen from Fig. 3 that as beta increases (with increasing time) the deposition profile becomes strongly peaked at the magnetic axis due to the outward shift of plasma. The deposition for one-half and one-third energy components (not shown in Fig. 3) is very poor for the 150 keV case. For the 200 keV beams, the 100 keV component peaks (at high  $\beta$ ) near the magnetic axis, however one-third energy component (67 keV) always remains an edge heating source.

The use of ICRF in TENTOK for bulk plasma heating to ignition (as well as possibly for current drive, impurity control, etc., which are not considered in the study) offers several advantages over neutral beams. In the frequency range of interest (30-100 MHz) efficient RF power sources are commercially available and RF systems appear to offer reduced capital and operating costs over the neutral beam systems, as well as improved reliability due to the fact that RF systems are less complex. The ICRF heating of TENTOK plasma to ignition involve the following scenario: (1) the minority species heating during the startup phase where the RF power is preferentially coupled to the minority ions which in turn heats the bulk plasma (majority ions) through collisions and (2) second-harmonic heating once the plasma is hot and dense (i.e., once the plasma beta reaches a finite value, several percent). A fixed frequency system is used in TENTOK for both minority and second harmonic heating schemes using rectangular waveguide launchers. The selected frequency  $f = 84$  MHz ( $\lambda/2 = 1.8$  m), which is the frequency corresponding to the second harmonic deuterium and the fundamental proton minority. A heating scenario with  $^3\text{He}$  minority ions in a deuterium plasma is also considered.

Using a cold plasma model, preliminary estimates of the ICRF launcher coupling efficiency indicate efficiencies in excess of 85% both for loop antennae and rectangular waveguide couplers. In the transport calculations, discussed in the previous section, this efficiency is assumed to be 75%.

In the TENTOK, refueling of the plasma is accomplished by controlled flow of deuterium and tritium in the form of a gas and frozen pellets. The injection of neutral particles (in the case of neutral beam heating) also provide fueling capability. A gas puffing system provides fueling (through both continuous and pulsed flow control) during the initial startup phase, and the pellet injectors provide fueling during the

plasma burn. Using a pellet fueling code (a subroutine PELLET extracted from the WHIST [3] code with a driver routine written specifically for TENTOK), specifications for the TENTOK pellet fueling system have been determined. The fuel burnup fraction and the time evolution of plasma density, temperature, and their profiles are important considerations in determining the pellet size, velocity, and repetition rate. The pellet sizes (radii) and velocities considered in the analysis are 2-4 mm and 2-4 km/s, respectively. Adequate fueling of plasma (especially when the full transport code is used) is found to be possible with 3 mm radius pellets at 2 km/s. Active fueling of more than 50% of the outer plasma volume is accomplished in this case.

#### Impurity Control and Particle Handling

Initial considerations of the impurity control, particle exhaust, and power handling system for TENTOK focused on the physical parameters of the two most explored concepts—pumped limiters and magnetic divertors. It was determined that both pumped limiters and poloidal (single- or double-null) divertors could handle the required particle and energy fluxes of a 3000 MW(t) reactor. Comparative assessments of these options, as well as the commercial nature of TENTOK, the reactor duty factor, reliability, and maintainability considerations outweighed capital cost considerations and a double-null poloidal divertor is chosen as the impurity control and particle handling system. Also, from a physics point of view a double-null configuration is more favorable than a single-null configuration. In a double-null configuration the scrape-off layer widths needed on the inboard and outboard sides are about equal because of the absence of a magnetic connection between the inboard and outboard scrape-off layers and the comparatively weak influx of particles and power into the inboard scrape-off layer. In the case of a single-null configuration, the magnetic connection between inboard and outboard sides leads (for  $\beta_p \sim 3$ ) to a requirement of about a three times larger scrape-off layer width on the inboard side than on the outboard side. Thus, a larger distance has to be kept between the plasma and the inner wall for a single-null divertor than for a double-null divertor, implying a poor use of available volume (valuable real estate). Also, in a single-null divertor the power distribution between the inboard and outboard divertor plates is about

one-to-one, whereas in a double-null divertor the power load is much smaller on the less accessible inboard plates (for example, in ASDEX out/in  $\approx 4/1$ ).

The double-null poloidal divertor system is located at the top and bottom of the toroidal plasma chamber. The equilibrium plasma configuration for this case is shown in Fig. 1(a). Preliminary analysis and modeling of plasma edge and divertor operation have been made. Results are discussed in Ref. [1].

### Diagnostics and Control

Preliminary considerations are given to the systems needed to diagnose and control the TENTOK to ensure successful operation. A narrative list of diagnostics proposed for the TENTOK is listed in Table III, which relate to measurement and/or control of (a) plasma poloidal beta, (b) impurity generation, and (c) fusion power. Discussions of these diagnostics are given in Ref. [1].

The computer system is an integral part of the controls and diagnostics for the TENTOK. While miniaturization of components present potential problems, an improvement in computing power by three orders of magnitude during the next 25-30 years is thought to be adequate, in most respects, for the control of this reactor. Such developments as speech generation and industrial robots should facilitate operation of the reactor. At the highest level, this computer system should be expected to simulate operation about 100 times as fast as real time. This requirement places a burden on theory and model development to become about 1000 times more efficient by the time the reactor is built.

### Acknowledgments

This study was carried out for partial fulfillment of the Plasma Engineering course taught by one of the authors (NAU) at the University of Tennessee. The authors would like to thank Drs. S. E. Attenberger, K. A. Houlberg, Y-K. M. Peng, and D. J. Strickler for valuable discussions and for making available many of the state-of-the-art computational tools used in this study. The support of the ORNL Fusion Energy Division, University of Tennessee Nuclear Engineering Department, and the Fusion Engineering Design Center are greatly appreciated.

References

- [1] K. E. Yokoyama et al., Plasma Engineering Studies for Tennessee Tokamak (TENTOK) Fusion Power Reactor, Oak Ridge National Laboratory report ORNL/TM-9002 (to be published).
- [2] C. C. Baker et al., STARFIRE-A Commerical Fusion Tokamak Power Plant Study, Argonne National Laboratory report ANL/FPP-80-1, 1980.
- [3] W. A. Houlberg, S. E. Attenberger, and L. M. Hively, "Contour Analysis of Fusion Reactor Performance," Nucl. Fusion 22, 935 (1982).
- [4] B. A. Carreras et al., "Transport Effects Induced by Resistive Ballooning Modes and Comparison with High  $\beta_B$  ISX-B Tokamak Confinement," Phys. Rev. Lett. 50, 503 (1983).
- [5] K. C. Shaing and J. D. Callen, "Neoclassical Ripple Transport in Tokamaks," Nucl. Fusion 22, 1061 (1982).
- [6] R. J. Hastie and W. N. G. Hitchon, "Energy Loss Due to Ripple Effects in INTOR," in G. Grieger et al., European Contributions to INTOR Phase-2A Workshop, EUR-FU-BRU/XII-2/81/EDV 70, Brussels (1982).

Table I. TENTOK Parameters

Geometry

Major radius, $R_0$	6.45 m
First wall radius, $a_w$	1.9 m
First wall surface area	680 m <sup>2</sup>
Blanket and shield thickness	1.5 m
Coil thickness	1.0 m

Plasma

Plasma radius, $a$	1.6 m
Plasma elongation, $\sigma$	1.65
Plasma triangularity, $\delta$	0.3
Plasma aspect ratio, $A$	4
Plasma volume, $V_p$	540 m <sup>3</sup>
Burn average beta, $\langle\beta\rangle$	6%
Poloidal beta, $\beta_p$	3.2
Average ion temperature, $\langle T_i \rangle$	15 keV
Average ion density, $\langle n_i \rangle$	$1.5 \times 10^{20} \text{ m}^{-3}$
Field on axis, $B_T$	5.6 T
Plasma current, $I_p$	8.5 MA
Energy confinement time, $\tau_E$	3 s
Safety factor, $q(a)$	2.5
Neutron wall loading, $P_w$	3 MW/m <sup>2</sup>
Fusion Power, $P_{fus}$	2500 MW
Total thermonuclear power, $P_{th}$ (blanket multiplication = 0.25)	3000 MW(t)

Heating - Neutral beam or RF

Beam power	125 MW
Beam energy	200 keV
RF frequency ( $\omega = 2\Omega_D$ )	84 MHz

Fueling - Pellet injection

Pellet radius	3 mm
Pellet velocity	2 km/s

Toroidal field coils

Number	12
Maximum field	$\leq 12$ T
Conductor	$Nb_3S_n, NbTi$
Bore	$8 \text{ m} \times 12 \text{ m}$
Peak-to-average ripple (edge)	1%

Impurity control

Method	double-null poloidal divertor
--------	-------------------------------

Table II. TENTOK Base Parameters and Models

Parameters (see Table I for complete list)

Peak-to-average ripple	
at inboard edge	0.4%
at outboard edge	1%
Deuterium beam energy	200 keV
Source species mix	80:12:8
Current mix to plasma	34:28:38
Beam injection geometry	perpendicular
Pellet radius and velocity	3 mm at 2 km/s

Models

Scrape-off	poloidal divertor
Fueling	pellet
Electron energy confinement	$\chi_e = 3 \chi_e^{NC} + 2 \chi_e^{an} + \chi_e^{CD}$
Ion energy confinement	$\chi_i = 3 \chi_i^{NC} + \chi_i^{RT} + \chi_i^{BD}$
Particle confinement	$D = 3D^{NC} + 2(0.2)\chi^{an}$
Fast alpha diffusion coefficient	1000 cm <sup>2</sup> /s
Impurities	none
Beam neutralization	ideal equilibrium fraction
RF heating profile	Gaussian

Table III. A short list of major plasma diagnostics for TENTOK

<u>Parameter</u>	<u>Diagnostic</u>
Plasma shape and position	$B_\theta$ loops, X-ray, plasma TV
Total plasma current and current profile	Rogowski loop, FIR
Density	Interferometer (FIR)
Fusion product power	Neutron activation foils
Voltage	Voltage loops
Beta measurement and and high- $\beta$ control	Diamagnetic loops and advanced diagnostics
Disruption precursors	X-ray imaging

### Figure Captions

Fig. 1. Equilibrium poloidal field contours (a) D-shaped plasma with double-null poloidal divertor ( $\langle\beta\rangle \approx 8\%$ ), (b) bean-shaped plasma ( $\langle\beta\rangle \approx 14\%$ ).

Fig. 2. Neutral beam (auxiliary) heating and fusion power contours for TENTOK with the reference transport model. Thermally unstable region, ignition, operating point, and optimal path are shown.

Fig. 3. Beam deposition profile for the full energy component as a function of time for (a) 150 keV and (b) 200 keV.

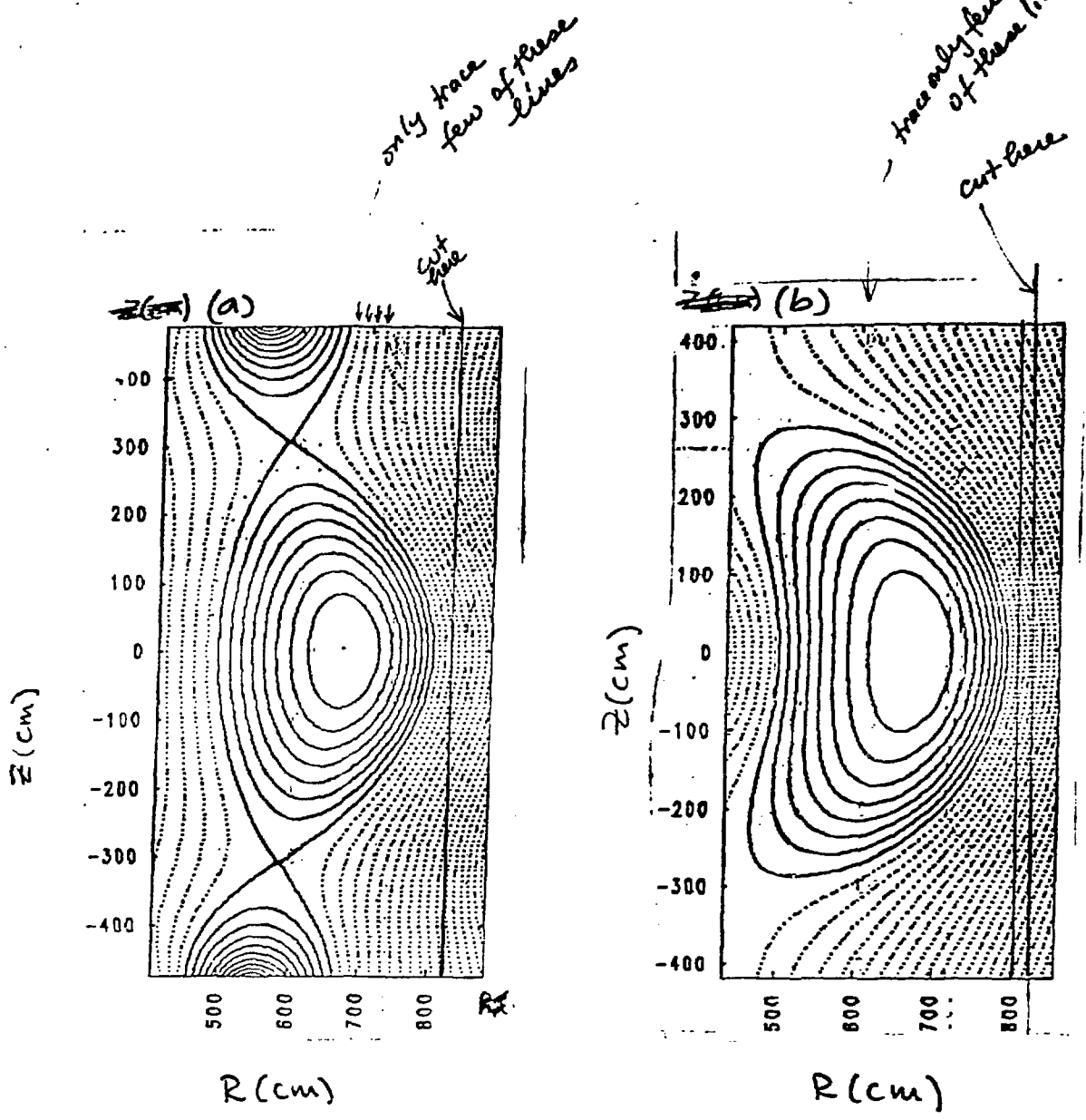
Fig. 4. TENTOK ICRF heating contours showing the ignition and thermally unstable region.

Fig. 5.  $Q$  contours and contours of average toroidal  $\langle\beta_T\rangle$  and poloidal  $\langle\beta_p\rangle$  beta including fast beam ion and fusion alpha pressure contributions. Ignition curve ( $Q = \infty$ ) and operating point are shown.

Fig. 6. Central ion and electron temperature contours. Ignition curve and operating point are superimposed.

Fig. 7. Total energy confinement time contours with ignition curve and operating point.

Fig. 8. TENTOK neutral beam power contours (in MW) for the reference model with  $D_\alpha = 1000 \text{ cm}^2/\text{s}$  (solid lines) and with  $D_\alpha = 5000 \text{ cm}^2/\text{s}$  (dashed lines).



Solid  
and dots or very short dashes.

Figure 1

Note  
Scales are  
somewhat  
different

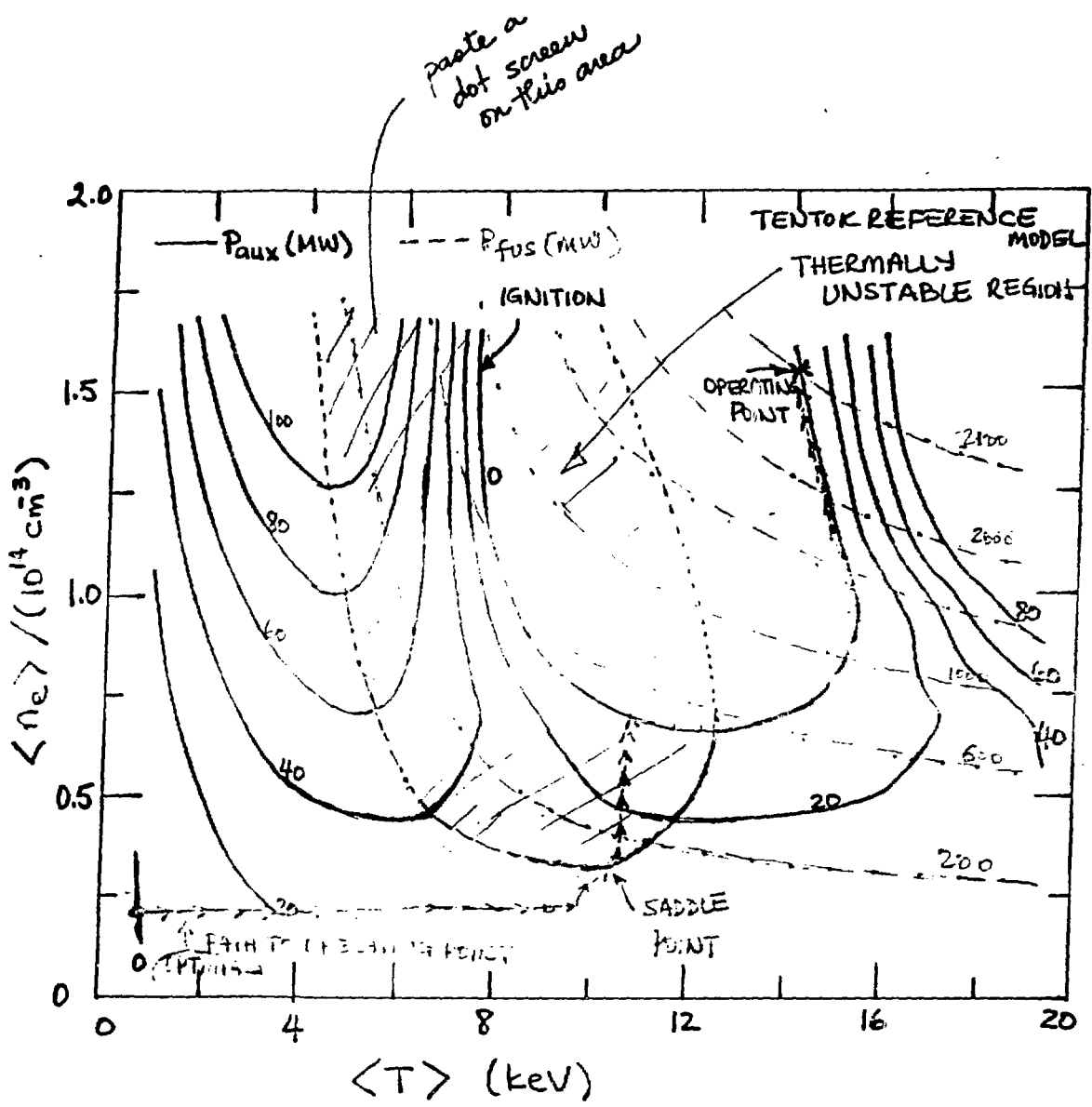


Figure 2

cleaner  
copy  
enclosed

124  
make two  
separate plots  
make copies  
of different  
copies

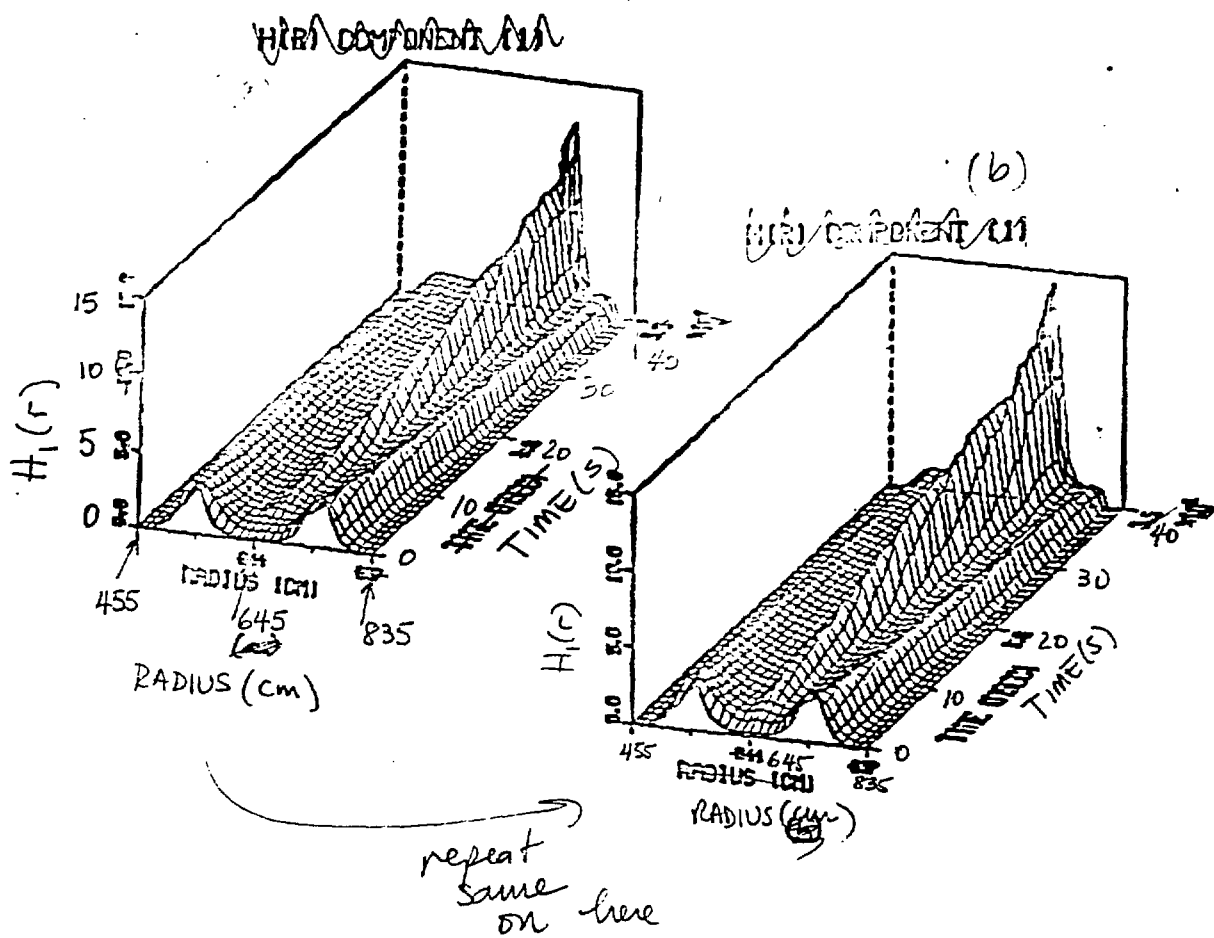


Figure 3: (a) 150 keV power deposition profile  
of full beam energy component in TENTOR  
(b) 200 keV power deposition profile  
of full beam energy component in TENTOR

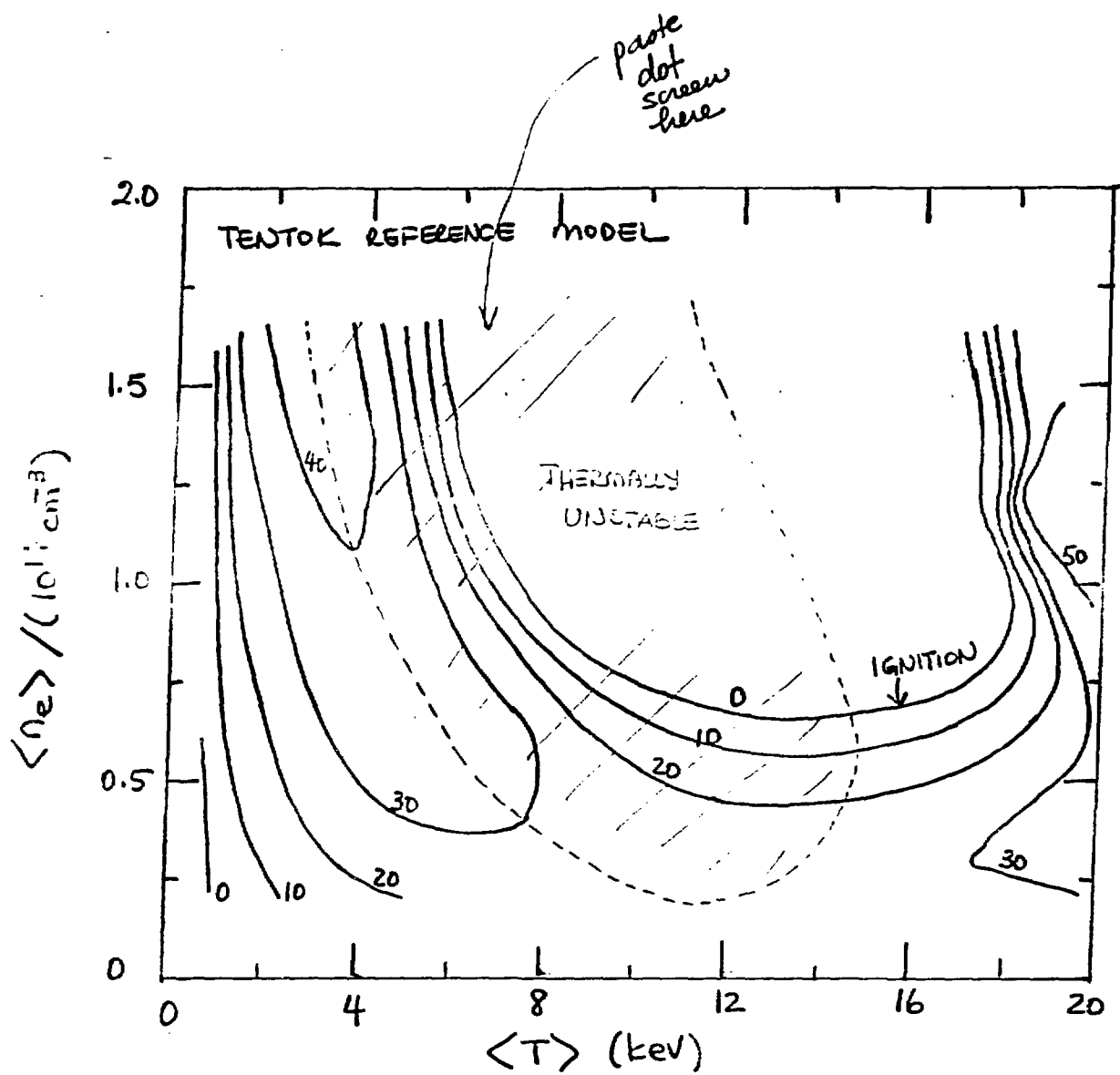
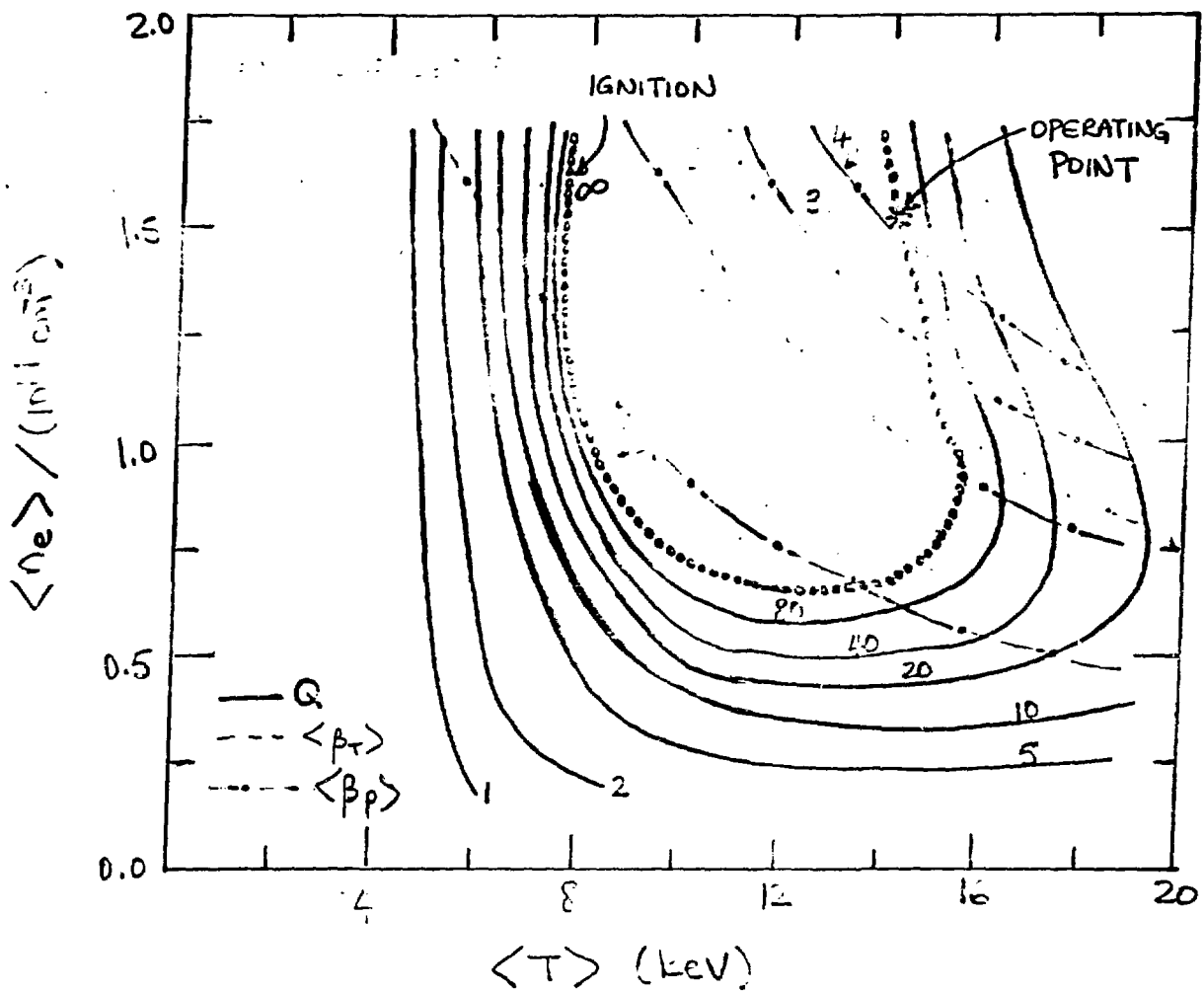


Fig. 4



F75

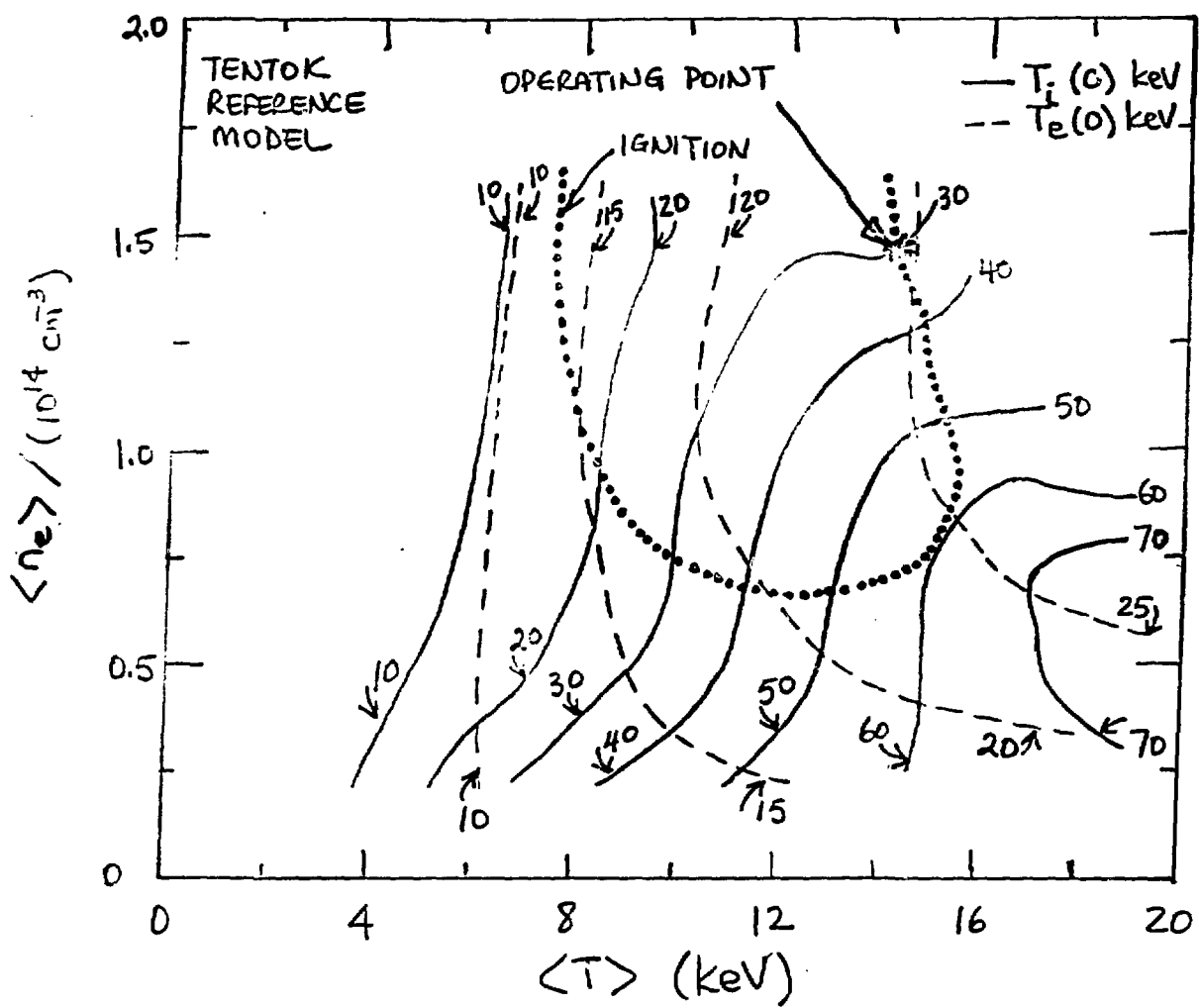


Fig 6

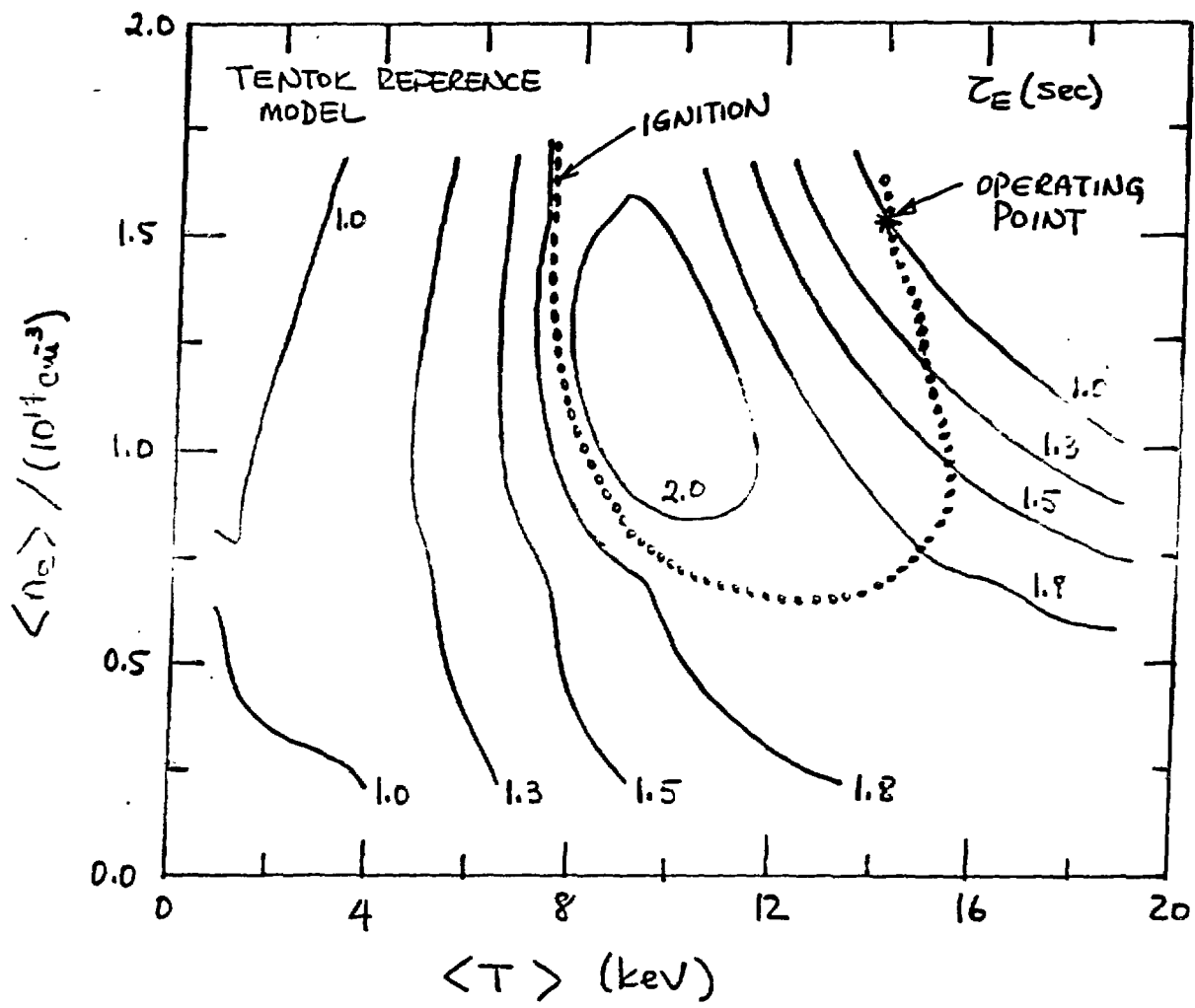


Fig 7

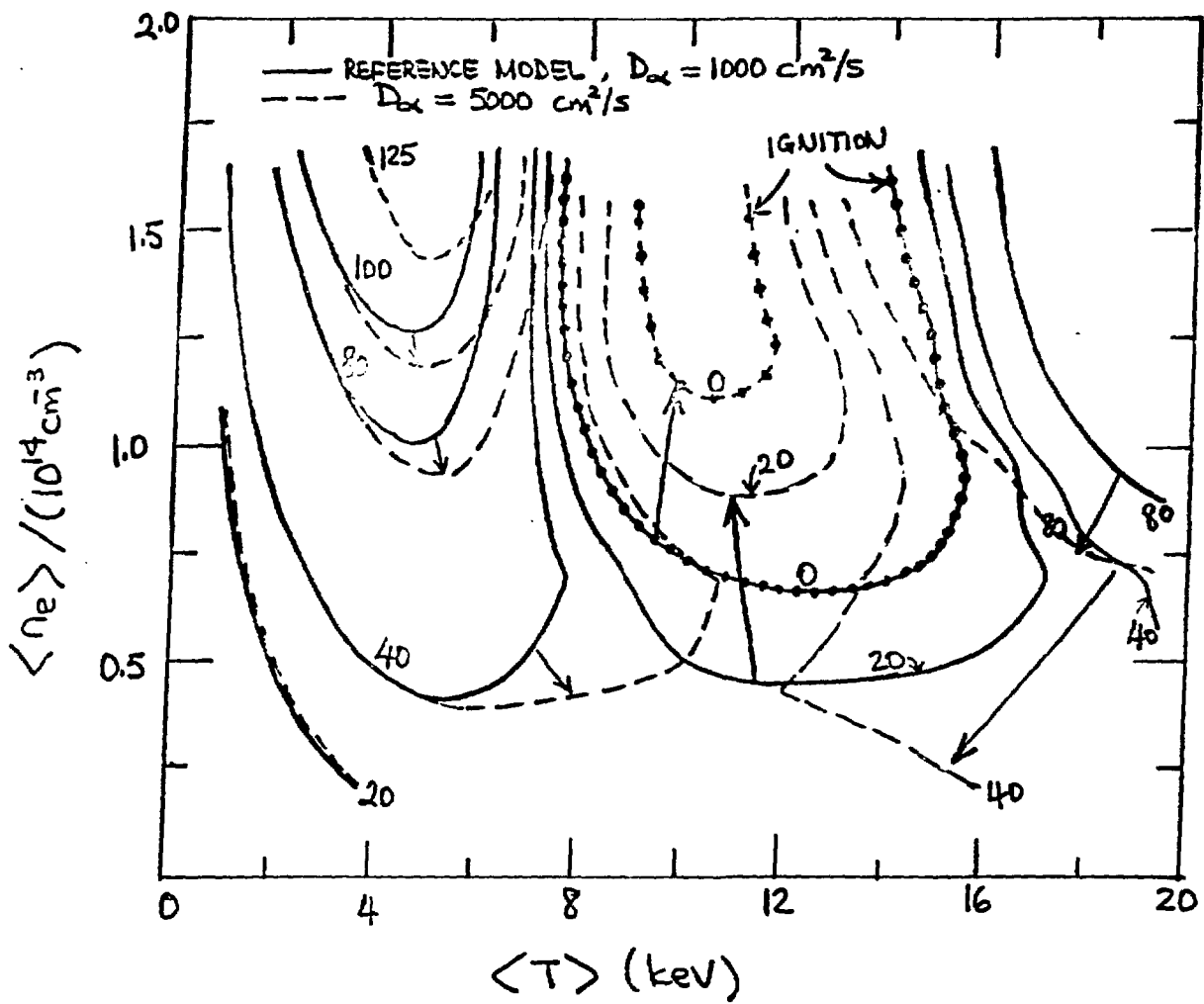


Fig 8